ACS APPLIED MATERIALS & INTERFACES

Research Article

www.acsami.org

Selective Growth of MoS_2 for Proton Exchange Membranes with Extremely High Selectivity

Kai Feng, Beibei Tang,* and Peiyi Wu*

State Key Laboratory of Molecular Engineering of Polymer, Department of Macromolecular Science and Laboratory of Advanced Materials, Fudan University, Shanghai 200433, People's Republic of China

Supporting Information

ABSTRACT: Proton conductivity and methanol permeability are the most important transport properties of proton exchange membranes (PEMs). The ratio of proton conductivity to methanol permeability is usually called selectivity. Herein, a novel strategy of *in situ* growth of MoS_2 is employed to prepare MoS_2/Nafion composite membranes for highly selective PEM. The strong interactions between the Mo precursor ($(NH_4)_2MoS_4$) and Nafion's sulfonic groups in a suitable solvent environment (DMF) probably lead to a selective growth of MoS_2 flakes mainly around the ionic clusters of the resultant MoS_2/Nafion composite membrane. Therefore, it would significantly promote the aggregation and hence lead to a better connectivity of these ionic clusters, which favors the increase in proton conductivity. Meanwhile, the existence of MoS_2 in the ionic channels effectively prevents methanol transporting through the PEM, contributing to the dramatic decrease in the methanol permeability. Consequently, the MoS_2/Nafion composite membranes exhibit greatly increased selectivity. Under some severe conditions, such as 50 °C with 80 v/v% of methanol concentration, an increase in the membrane selectivity by nearly 2 orders of magnitude compared with that of the recast Nafion membrane could be achieved here, proving our method as a very promising way to prepare high-performance PEMs. All these conclusions are confirmed by various characterizations, such as (FE-) SEM, TEM, AFM, IR, Raman, TGA, XRD, *etc.*

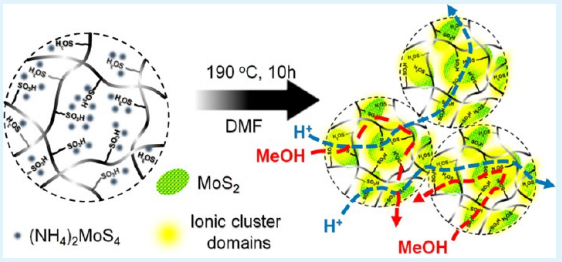

KEYWORDS: *proton exchange membrane, molybdenum disulfide, Nafion, selective growth, high selectivity*

1. INTRODUCTION

The urgent desire for renewable and clean sources of electric power has inspired great enthusiasm for the research on fuel cell in the recent years.[1,2] Direct methanol fuel cell (DMFC), classified as the sixth fuel-cell type,[3,4] has received considerable research interest due to its great potential as an environmentally benign energy conversion device for mobile and portable power applications.[5−8] A crucial building block of DMFC is the proton exchange membrane (PEM), which should ideally allow for only proton transportation, no methanol crossover, from anode to cathode,[1,9−11] because any methanol crossover to the cathode would inevitably decrease the cell potential and in turn significantly reduce the overall fuel efficiency.[3] However, despite the fact that intensive efforts have been paid to develop a cornucopia of alternative approaches to minimize the methanol crossover, such as incorporating various organic and/or inorganic materials into the membrane matrix,[5,12−16] it is still a big challenge for the wide commercialization of DMFCs.[1,12] Take Nafion for example: it is one of the typical PEMs currently used for DMFCs due to its high proton conductivity and excellent chemical resistivity, thermo-mechanical stability as well as durability under dynamic operation conditions.[12−14,17−19] It is comprised of a polytetrafluoroethylene backbone with perfluoroether side chains bearing terminal sulfonic groups, resulting in a unique bicontinuous microstructure of the hydrophobic backbone and the hydrophilic ionic clusters.[12,16,20] Generally, good connectivity of these ionic clusters would facilitate the hopping of protons through the membrane and hence bestow excellent proton conductivity upon the Nafion-based PEMs.[16,21,22] However, under this circumstance, severe methanol crossover also exists for both of them transport almost through the same path (ionic channels) inside the Nafion matrix. Sometimes, researchers have to reduce the methanol crossover at the expense of the proton conductivity.[12] Therefore, the decrease in methanol crossover with the enhancement or at least maintenance of the proton conductivity for highly selective PEMs is quite difficult to achieve.[1]

Since the rise of graphene in 2007,[23] research attempting to take full advantage of the fascinating properties, such as high specific area, barrier effect, and good thermo-mechanical stability, of two-dimensional (2D) layered materials has been triggered recently to develop novel high-performance polymer-based materials.[24−34] The already-obtained achievements have also proved their great potential for practical applications in the field of PEMs.[5,12,13,16,35] Understandably, the dispersion of these 2D materials inside the polymer matrix, which greatly affects the performance of the resultant materials, is always the

Received: September 11, 2013
Accepted: November 27, 2013
Published: November 27, 2013

major concern during the preparation process.[16,25,28] Until now, only the PEMs modified by (functionalized) graphene oxide (GO) are intensively investigated. GO's good dispersibility inside the Nafion matrix derives from its own abundant hydrophilic functional groups. It benefits the water retention capability of PEMs and probably could reorganize their ionic channels, thus enhancing the membrane conductivity under increased temperature and/or low humidity.[13,16] However, many other important 2D compounds, such as transition metal dichalcogenides (TMDs), transition metal oxides (TMOs), and BN, Bi_2Se_3 and *etc.*, have long attracted much less attention.[25] Unlike GO or other traditional hygroscopic inorganic additives, such as TiO_2, SiO_2, and ZrO_2,[5] their practical applications are always hampered by the shortage of functional groups and hence the lack of a facile method to disperse them stably in common solvents in a large quantity.[25] Furthermore, such a shortage of functional groups seemingly provides an illusion that they may be useless in the applications on ionic conductors, or PEMs, to put it more specifically. Therefore, to the best of our knowledge, scant investigation has been conducted into the TMD/TMO modified PEMs.

Among these TMDs and TMOs, MoS_2 is one of the most attractive and commonly investigated as a catalyst for hydrodesulfurization[28,36] and hydrogen evolution.[37−41] It is composed of hexagonal layers of Mo atoms sandwiched between two layers of S atoms, resulting in a similar structure with graphene.[25] Herein, an approach of selective formation of MoS_2 inside the Nafion matrix is employed. The strong interactions between the Mo precursor ($(NH_4)_2MoS_4$) and Nafion's sulfonic groups in a suitable solvent environment (DMF) probably lead to the selective growth of MoS_2 flakes mainly around the ionic clusters of the resultant MoS_2/Nafion membrane.[36,42,43] It promotes the aggregation and hence leads to a better connectivity of these ionic clusters, which favors the increase in proton conductivity. Meanwhile, the existence of MoS_2 flakes in those ionic channels effectively prevents methanol transporting through the membrane, contributing to the dramatic decrease in methanol permeability. Accordingly, MoS_2/Nafion composite membranes for PEMs with extremely high selectivity are obtained in this study. Actually, such a strategy applies equally for other TMDs or TMOs, for example, WS_2,[44] offering new degrees of freedom to prepare high-performance PEMs modified by various 2D materials.

Besides, based on the former experimental experiences of our group,[44−48] a distinctive technique, real-time attenuated total reflection Fourier transform infrared (ATR-FTIR), is introduced in this study to investigate the methanol permeability of these PEMs. This *in situ* method can overcome several problems associated with traditional "blot and weigh/measure" immersion techniques and is especially powerful for the analysis of liquid diffusion in polymers.[46,49] It has hitherto been widely used in the investigations on the diffusion of penetrants that are responsive to infrared,[45−53] including methanol.[54−56] Herein, our experimental results find that the ATR-FTIR technique could promptly and easily obtain the methanol permeability of these composite membranes. Therefore, we believe that it could be a potential general method in the field of PEMs.

2. EXPERIMENTAL SECTION

2.1. Materials. Nafion solution (perfluorinated resin solution, 5 wt % in lower aliphatic alcohol and water mixture) was purchased from DuPont. $(NH_4)_2MoS_4$ was provided by Sigma Aldrich. Unless otherwise stated, all the other reagents were obtained from the commercial suppliers and used without further purification.

2.2. Preparation of the MoS_2/Nafion Composite Membranes and the MoS_2+Nafion Blending Membranes. First, a Nafion/DMF solution was obtained by completely replacing the solvent of 4 mL as-received Nafion solution with DMF via the method that is almost similar to our former work.[16] Then, the precursor $(NH_4)_2MoS_4$ was added into the Nafion/DMF solution in an amount that would give the reduced MoS_2 with a content in the range of 0.1−1 wt %. The mixture was stirred and ultrasonicated for 0.5 h to help $(NH_4)_2MoS_4$ disperse well before the treatment at 190 °C for 10 h.[36] It is in the solvothermal process that $(NH_4)_2MoS_4$ was reduced into MoS_2.[36] Second, the obtained MoS_2/Nafion/DMF mixture was carefully casted into a 2 cm × 5 cm rectangular model. The detailed information about the following preparation procedures, such as the membrane formation by evaporating DMF and then converting the membrane into H^+ form, can be obtained from our previous work.[16] All these membranes prepared via the procedures described above are called "0.1−1 wt % MoS_2/Nafion composite membranes". Furthermore, another different kind of PEM, named "MoS_2+Nafion blending membrane", was prepared by simply adding MoS_2 powder into the Nafion/DMF solution and then sonicating the resultant mixture for 24 h before the casting step. Its subsequent treatment process was similar with that of the MoS_2/Nafion composite membranes. The detailed schematic illustration of all these preparation procedures can be obtained from Supporting Information Figure S1.

2.3. Membrane Characterizations. Both the surface and the cross-sectional morphologies of these PEMs, including the MoS_2/Nafion and the MoS_2+Nafion membranes, were observed with a SEM (scanning electron microscopy, XL 30 ESEM-TMP PHILIP). All the samples were coated with gold before the SEM observation. The cross-sectional TEM (transmission electron microscopy) images, conducted on a JEOL JEM2100 TEM instrument operated under an acceleration voltage of 200 keV, were also obtained to investigate the dispersion of MoS_2 inside the PEMs. The AFM (atomic force microscopy) measurements were recorded by using a Multimode Nano 4 in the tapping mode. XRD (X-ray diffraction, PANalytical X'pert diffractometer with Cu Kα radiation) was employed to characterize the effects of MoS_2 on the membrane microstructures. The FT-IR (Fourier transform infrared spectroscopy) characterization was carried out on a Nicolet Nexus 470 spectrometer with a resolution of 4 cm^{-1} and 64 scans, and the TGA (thermogravimetric analysis) was performed under N_2 atmosphere at a heating rate of 10 °C min^{-1} by a Perkin-Elmer Thermal Analyzer. The Raman spectra were collected on a Renishaw inVia Reflex micor-Raman spectrometer with 633 nm laser excitation.

The proton conductivities of these PEMs under different conditions were obtained via the same method reported in our former work.[16] Their methanol permeability was measured under 25 and 50 °C with the aid of the homemade equipment schematically illustrated in Figure 1. First, a dry membrane was put onto the ZnSe crystal in the ATR cell (Nicolet Nexus 470 FTIR spectrometer) and then sandwiched between the crystal and the PTFE mold. Second, the continuous data were obtained as soon as 0.5 mL of 80 v/v% methanol/H_2O

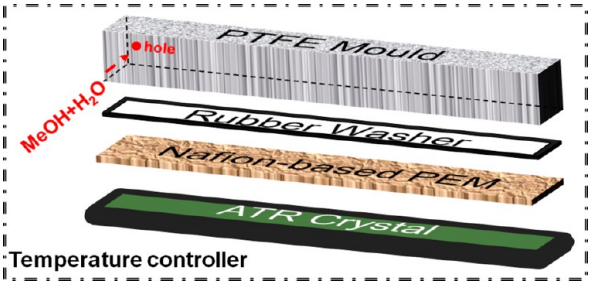

Figure 1. Schematic illustration of the homemade equipment used to characterize the methanol permeability through these PEMs.

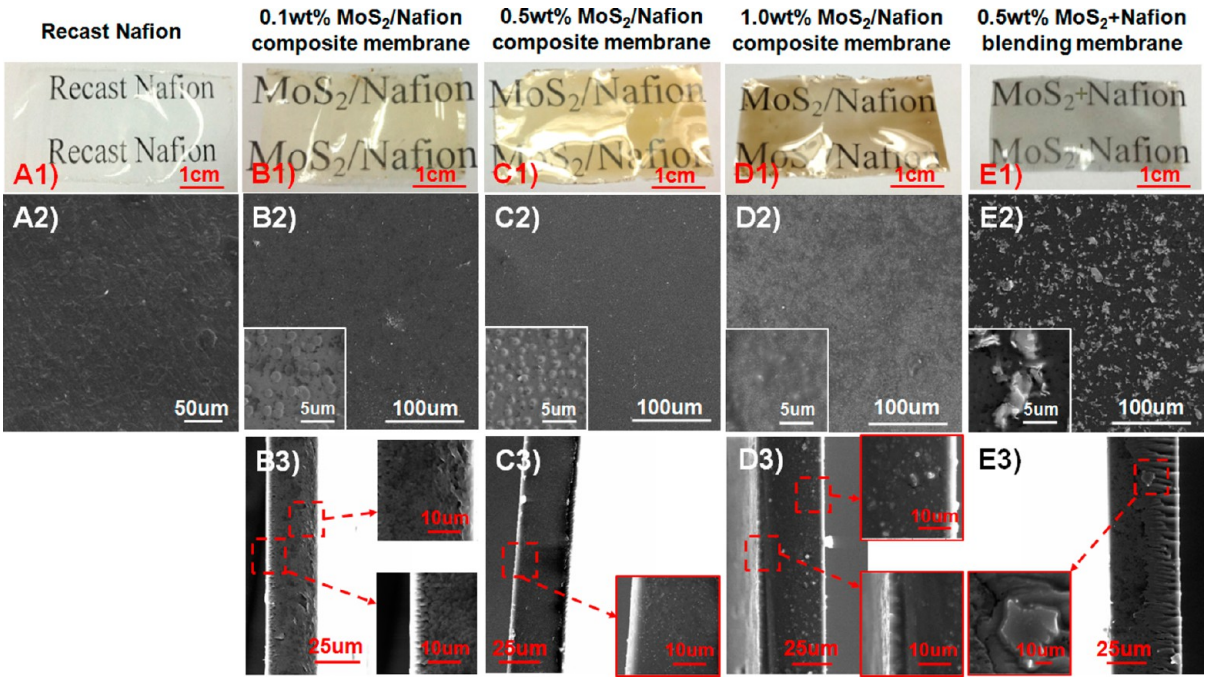

Figure 2. Digital photos (A1−E1) and surface SEM images (A2−E2) of the recast Nafion membrane,[16] the 0.1−1.0 wt % MoS_2/Nafion composite membranes, and the 0.5 wt % MoS_2+Nafion blending membrane; Cross-sectional SEM images (B3−E3) of the 0.1−1.0 wt % MoS_2/Nafion composite membranes and the 0.5 wt % MoS_2+Nafion blending membrane; one or two more SEM images at a higher resolution are shown in the corresponding insets of B2−E2 and B3−E3.

solution was injected into the PTFE mold through the little hole with the aid of an injector. The little hole was blocked during the entire measurement to avoid any evaporation of methanol. The data, based on 4 cm^{-1} spectral resolution, were taken as a function of diffusion time with acquisition time interval of 40 s by using a macro-program. Third, according to the increase in the peak area corresponding to the $-CH_3$ stretching vibration, the diffusion coefficients of methanol in these PEMs were calculated from the Fickian diffusion equation put forward by Fieldson and Barbari.[57] Detailed calculation process can be found in our already-published work.[45]

3. RESULTS AND DISCUSSION

As the digital photos shown in Figure 2A1−E1, it seems that both of these two preparation approaches, including the selective formation of MoS_2 and simply adding pristine MoS_2 into the membrane matrix (Supporting Information Figure S1), could obtain uniform PEMs. However, interestingly in Figure 2C1, E1, with the same amount of MoS_2 being incorporated into the Nafion matrix, the 0.5 wt % MoS_2/Nafion composite membrane and the 0.5 wt % MoS_2+Nafion blending membrane exhibit totally different colors. The former one is chalky yellow, while the latter shows greyish. This phenomenon parallels Coleman's discovery that only the system containing well dispersed MoS_2 with small sizes is yellow.[58] The magnified observation by the surface SEM characterization in Figure 2A2−E2 (including Supporting Information Figures S2−S4) presents the obvious aggregation of MoS_2 flakes in the 0.5 wt % MoS_2+Nafion blending membrane, despite the fact that the MoS_2/Nafion/DMF mixture had been ultrasonicated for 24 h during its aforesaid preparation process (Supporting Information Figure S1B). While for the 0.1−0.5 wt % MoS_2/Nafion composite membranes, nanosized MoS_2 flakes are embedded randomly and tightly inside the membrane matrix, demonstrating that the selective-growth approach could bestow the excellent MoS_2 dispersion upon the composite membranes (Figure 2C2, C3 and Supporting Information Figure S3). This phenomenon is further confirmed by the cross-sectional TEM images in Figure 3A, B. Clearly, the poor dispersion of MoS_2 in

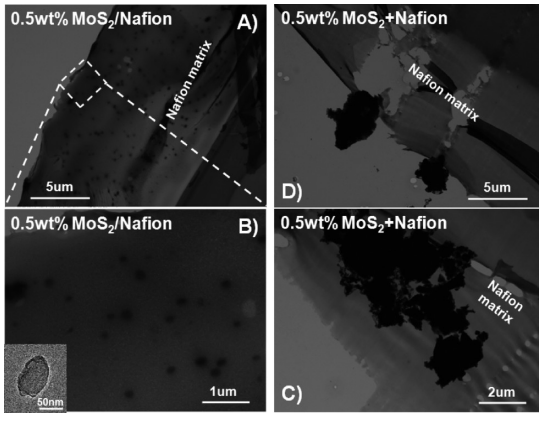

Figure 3. Cross-sectional TEM images of the 0.5 wt % MoS_2/Nafion composite membrane (A, B) and the 0.5 wt % MoS_2+Nafion blending membrane (C, D). The TEM image of the 0.5 wt % MoS_2/Nafion composite membrane at a higher resolution is shown in the inset of B.

the 0.5 wt % MoS_2+Nafion blending membrane (Figure 3C) would lead to its weak interactions with the Nafion polymer chains and hence its bad compatibility with the membrane matrix (Figure 3D). Honestly, there are already some relatively small aggregations of MoS_2 in the 1.0 wt % MoS_2/Nafion composite membrane (Figure 2D2 and D3). It is probably because of the increase in both of the quantity and the size of MoS_2 inside the membrane matrix.[58] It indicates that further increasing the amount of MoS_2 would greatly damage its dispersion even through the selective formation (an *in situ* approach). Large aggregations of MoS_2 could be found in the

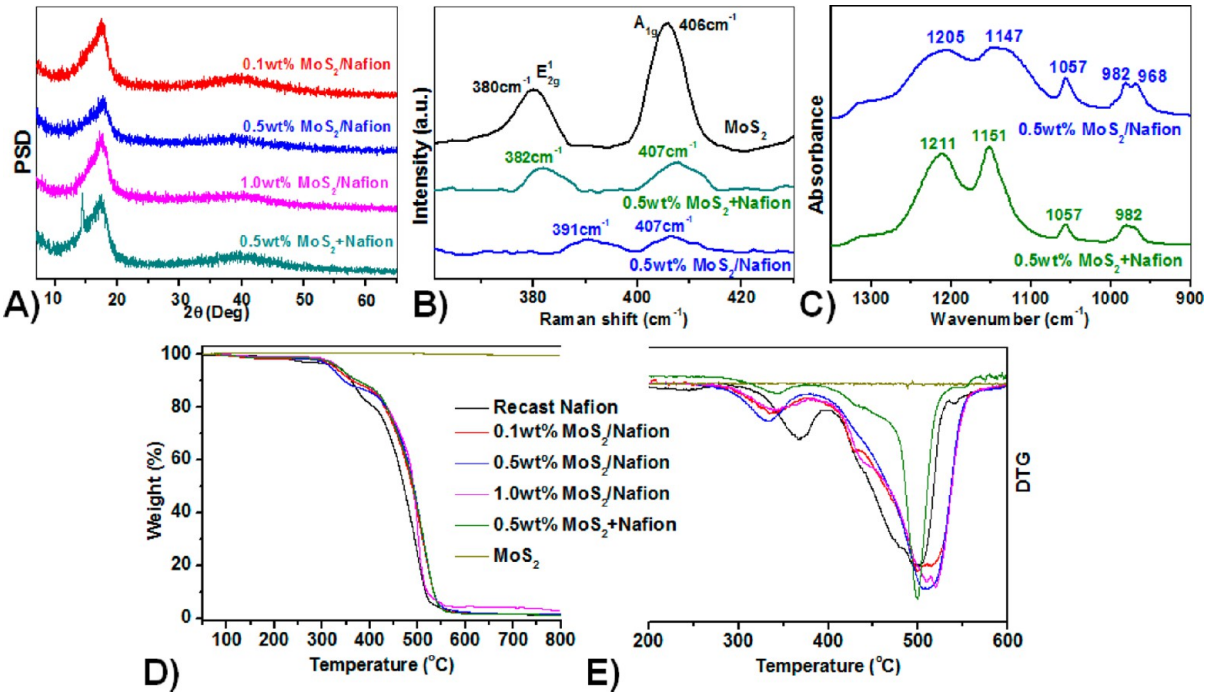

Figure 4. (A) XRD patterns and (C) IR spectra of the MoS_2/Nafion composite membranes and the 0.5 wt % MoS_2+Nafion blending membrane. (B) Raman characterizations of the pristine MoS_2, the 0.5 wt % MoS_2/Nafion composite membrane and the 0.5 wt % MoS_2+Nafion blending membrane. (D, E) TGA analyses (10 °C min^{-1}, N_2) of the recast Nafion membrane,[16] the MoS_2/Nafion, and the MoS_2+Nafion membranes.

2.0 wt % MoS_2/Nafion composite membrane, as the surface SEM images present in Supporting Inforamtion Figure S5A–C.

Normally, Nafion's bicontinuous microstructure derives a diblock morphology in its cross-sectional SEM image.[16] Whereas with MoS_2 being incorporated into the membrane matrix within a proper quantity via the selective-growth approach, such a morphology becomes less evident (Figure 2B3, C3) and even an almost uniform one is observed in the 0.5 wt % MoS_2/Nafion composite membrane (Figure 2C3). This compatibility effect could be attributed to the strong interfacial interactions of MoS_2 with both the backbone domains and the ionic cluster domains of Nafion. It is also confirmed by the XRD results (Figure 4A) that the peak intensity, in proportion to the electron-density difference between the ionic cluster domains and the backbone domains,[12,16] is obviously weakened when the quantity of MoS_2 increases from 0.1 wt % to 0.5 wt %. Noteworthily, when a higher amount of MoS_2 is employed, such as the 1.0 wt % MoS_2/Nafion composite membrane described above, these interactions would become weaker probably because of the aggregation of MoS_2. Interestingly but understandably, a characteristic peak around 2θ = 14.3°, corresponding to the (002) reflection of the *c* axis of large MoS_2 flakes (Supporting Information Figure S2B),[44] is found in the XRD pattern of the 0.5 wt % MoS_2+Nafion blending membrane in Figure 4A. This stacking phenomenon among these MoS_2 layers exactly demonstrates the poor dispersion of MoS_2 inside the membrane prepared by the conventional solvent blending method (Figure 2E2 and E3). The discovery that no typical XRD peak for MoS_2 emerges in the XRD patterns of the 0.1–1.0 wt % MoS_2/Nafion composite membranes could be attributed to (1) the good dispersion of MoS_2 (i.e. no stacked MoS_2 flakes existing in the MoS_2/Nafion composite membranes) and (2) the low MoS_2 content. The characteristic XRD peak corresponding to MoS_2 nanoplatelets[59] could be found around 16° in the XRD pattern of MoS_2/Nafion composite membrane with higher MoS_2 contents (for example, the 2.0 wt % MoS_2/Nafion membrane as shown in Supporting Information Figure S5D).

Figure 4B presents the Raman spectra of MoS_2 and the 0.5 wt % MoS_2+Nafion blending membrane as well as the 0.5 wt % MoS_2/Nafion composite membrane. The pristine MoS_2 shows the distinct band features (i.e., 380 cm^{-1} arising from the E^1_{2g} vibration and 406 cm^{-1} from the A_{1g} vibration).[26] Obviously, only the 0.5 wt % MoS_2/Nafion composite membrane gives largely shifted Raman bands, proving the existence of strong interactions between Nafion polymer chains and MoS_2.[9] Meanwhile, from the perspective of membranes via the FTIR characterizations displayed in Figure 4C (Supporting Information Figure S2C), similar results could also be obtained from the broadening and/or shifting phenomenon of the following IR bands compared with those of the recast Nafion.[12,16,60] The two weak peaks at 970 and 982 cm^{-1} are attributed to the symmetric stretching of the −COC− groups of Nafion polymer, while those at 1055 cm^{-1} and 1151 cm^{-1} are ascribed to the symmetric stretching vibrations of the $-SO_3^-$ and $-CF_2-$ groups, respectively.[60] The superimposed absorption band, corresponding to the asymmetric stretching vibrations of both the $-SO_3^-$ and $-CF_2-$ groups, occurs around 1213 cm^{-1}.[60] Actually, the conventional solvent blending method would also disperse very tiny amount of MoS_2 flakes well inside the membrane matrix, which nevertheless has little influence on the membrane performance, as the much weaker interactions between these MoS_2 and the Nafion matrix indicated by the XRD, Raman and FTIR measurements of the 0.5 wt % MoS_2+Nafion blending membrane (Figure 4A–C).

The TGA analyses of these PEMs (Figure 4 D, E) show that with 0.1–0.5 wt % MoS_2 being incorporated via the selective-growth approach, the desulfonation process in the range 250–400 °C shifts obviously toward lower temperature, while the

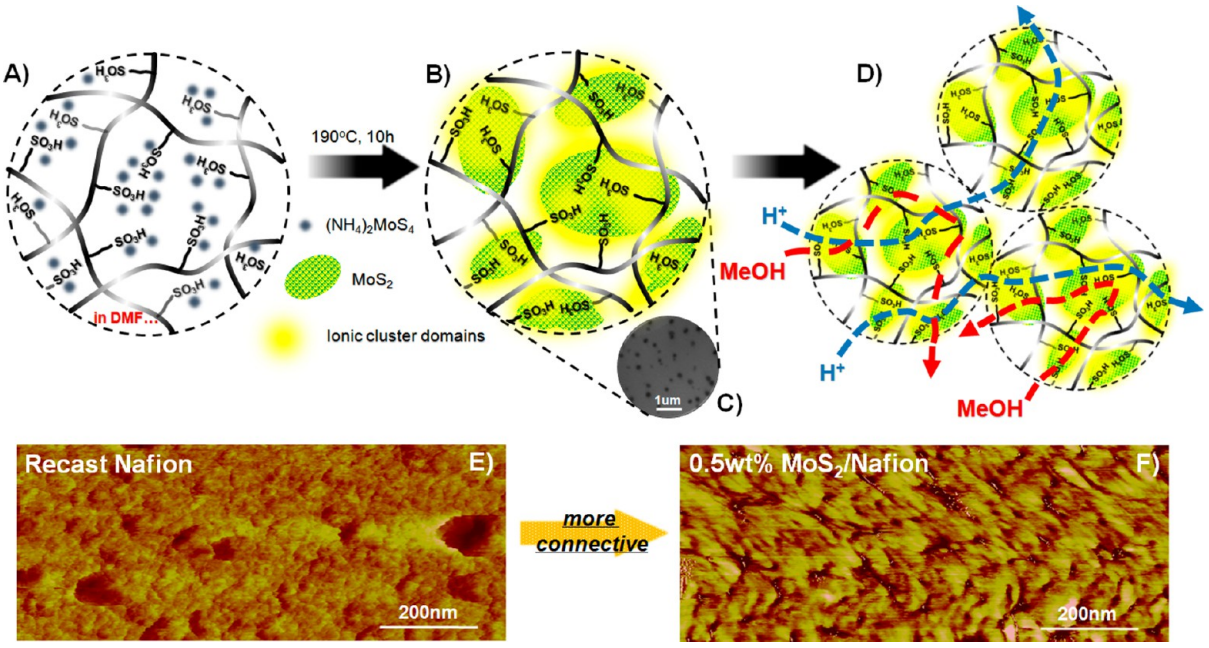

Figure 5. (A/B/D) The mechanism of the selective growth of MoS_2 mainly around the ionic cluster domains inside the membrane matrix. (C) Cross-sectional TEM image of the 0.5 wt % MoS_2/Nafion composite membrane. (E, F) AFM phase images of the recast Nafion membrane and the 0.5 wt % MoS_2/Nafion composite membrane.

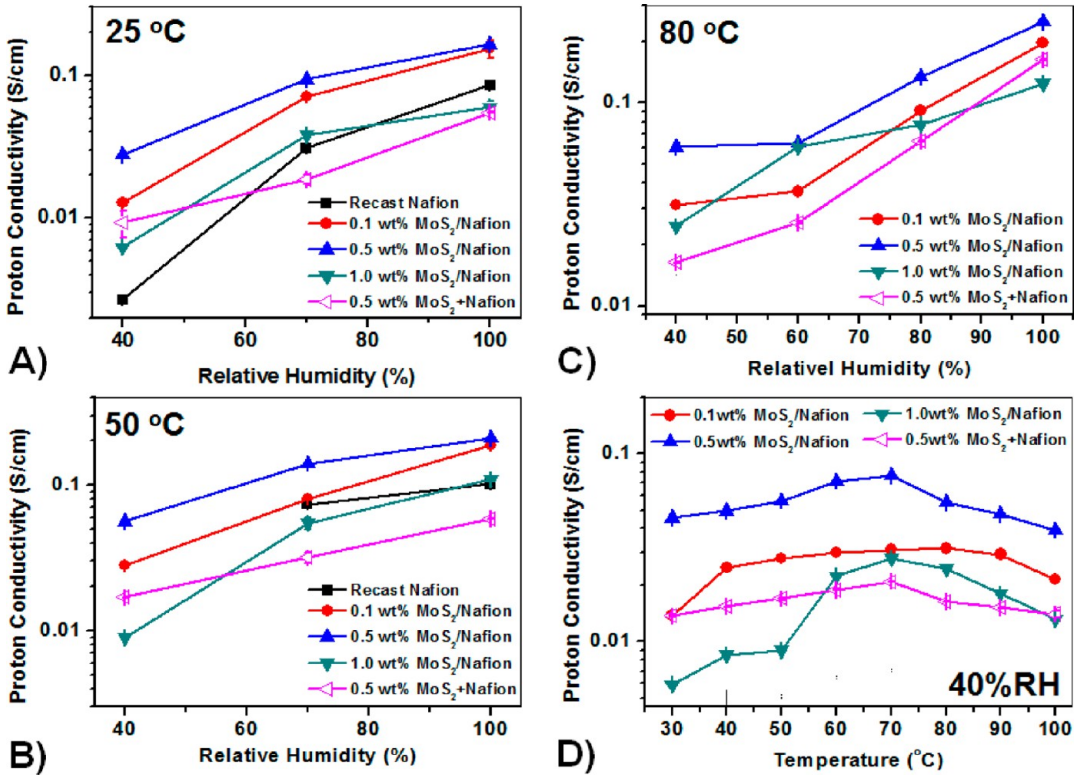

Figure 6. (A–C) Humidity-dependent proton conductivity plots (25, 50, and 80 °C) and (D) temperature-dependent proton conductivity plots (40% RH) of the recast Nafion membrane,[16] the 0.1–1.0 wt % MoS_2/Nafion composite membranes and the 0.5 wt % MoS_2+Nafion blending membrane.

backbone decomposition temperature around 500 °C increases slightly.[12] The former experimental result indicates that incorporating MoS_2 into the Nafion matrix via the selective-growth approach could make the sulfonic groups much more flexible, which would strongly benefit the enhancement of proton conductivity.[61] Furthermore, it is also consistent with Hong's discovery that smaller ionic cluster domain has relatively higher desulfonation temperature compared to that of the recast Nafion membrane.[12] As schematically illustrated in Figure 5A–D, MoS_2 would mainly grow around the ionic cluster domains due to the strong interactions between the Mo precursor $(NH_4)_2MoS_4$ and the hydrophilic sulfonic groups in a

suitable solvent environment (DMF).[36] As we had anticipated, it probably promotes the aggregation and hence leads to a better connectivity of these ionic clusters, as confirmed by the AFM phase images of the recast Nafion membrane and the 0.5 wt % MoS_2/Nafion composite membrane in Figure 5E, F (including Supporting Information Figure S6). The comparatively lighter parts are assigned to the softer hydrophilic ionic clusters while the darker ones correspond to the neutral hydrophobic backbone domains of the membrane.[16,21,62] Generally, both the size and the connectivity of these ionic cluster domains play important roles in the membrane conductivity. A much more connective network of ionic clusters would intensively facilitate the proton transport in the PEMs.[16,61−63]

Apparently, in both Figure 5E, F and Supporting Information Figure S6, the 0.5 wt % MoS_2/Nafion composite membrane has much larger ionic cluster domains of various sizes and better connectivity, which positively influences its conductivity improvement (Figure 6). As is well-known, the proton conduction in Nafion matrix is mainly governed by two mechanisms: the "proton hopping" (Grotthus) mechanism and the migration of hydrated protons ($H^+(H_2O)_n$). Understandably, there will be a larger amount of H_2O available for both the hopping mechanism and solvating protons for migration under higher RH conditions. This is exactly why the proton conductivities of the recast Nafion, the MoS_2/Nafion, and the MoS_2+Nafion membranes stably increase with RH increasing. However, there are large differences in the RH dependence in proton conductivity of these PEMs, as shown in Figure 6A. We believe that this phenomenon mainly comes from the difference in the contribution ratio of these two conduction mechanisms to the total proton conductivity when different amount of MoS_2 is incorporated into the Nafion matrix via different approaches. Take the selective approach (Suppporting Information Figure S1A) for example: it could lead to a good connectivity of the ionic clusters, which facilitates the hopping of protons. However, under this circumstance, the increased tortuosity caused by the existence of MoS_2 along the ionic channels would inhibit not only the methanol transportation but also the migration of hydrated protons, which is unfavorable for the enhancement of proton conductivity. To put it more specifically, compared with the 0.1 wt % MoS_2/Nafion composite membrane, the 0.5 wt % one has a better connectivity of the ionic clusters but increased tortuosity. In other words, probably the contribution ratio of the "hopping mechanism" to the proton conductivity of the 0.5 wt % MoS_2/Nafion composite membrane is relatively larger than that of the 0.1 wt %, resulting in a different RH dependence in proton conductivity.

Besides, the performance enhancement is much more evident especially under the low-humidity conditions (Figure 6D). Generally, the proton conductivity would increase with the temperature increasing. However, the decreasing phenomenon of proton conductivity of the Nafion-based PEMs at higher temperature is also often found because of the fast evaporation of water and hence the great loss of water inside the membrane matrix. This is also why the change of proton conductivity against temperature is unstable in Figure 6D. Usually, the proton conductivity of the recast Nafion membrane starts to decrease around 85 °C,[13,16] while only around 75 °C for both the MoS_2/Nafion and the MoS_2+Nafion membranes (Figure 6D). This discovery could be probably attributed to the hydrophobic nature of the incorporated MoS_2 which is benefit for the evaporation of H_2O at higher temperature.

In the case of 0.5 wt % MoS_2+Nafion blending membrane, the advantage, such as that of the selective-growth approach, almost disappears. Moreover, an even lower proton conductivity compared to that of the recast Nafion membrane is observed under some conditions (such as 80 °C-60%RH, Figure 6C), probably because MoS_2 itself is an insulator for proton. Besides, the aggregation of MoS_2 inside the 1.0 wt % MoS_2/Nafion composite membrane has negative effects on the improvement of its proton conductivity compared with that of the 0.5 wt % one (Figure 6).

Generally, harsh operation conditions, such as high methanol concentration and/or increased temperature, would leads to high methanol permeability of PEMs. Among these composite membranes, the 0.1 and 0.5 wt % MoS_2/Nafion membranes present obviously increased selectivity, as demonstrated in Table 1 and Figure 7. Under 50 °C with 80 v/v% of methanol concentration, even an increase in the selectivity by nearly 2 orders of magnitude compared with that of the recast Nafion membrane could be achieved, indicating the MoS_2/Nafion composite membrane as a very promising candidate for highly selective PEMs. It can be rationalized by the existence of MoS_2 along the ionic channels and hence the increased tortuosity of the membrane, which suppresses the methanol transportation through the membrane, and the significant improvement of its proton conductivity, which results from the more connective ionic cluster domains (Figure 5D). All in all, it proves that the selective-growth strategy is a very effective way to prepare low methanol-crossover PEMs in conjunction with excellent proton conductivity.

Table 1. Methanol Permeability of the Recast Nafion Membrane, the 0.1−1.0 wt % MoS_2/Nafion Composite Membranes, and the 0.5 wt % MoS_2+Nafion Blending Membrane

	permeability (P, × 10^{-9} cm^2 s^{-1})			
PEMs	25 °C		50 °C	
recast Nafion	30.58	±1.80	109.81	±19.74
0.1 wt % MoS_2/Nafion	4.62	±0.24	10.87	±0.68
0.5 wt % MoS_2/Nafion	8.31	±0.45	14.01	±0.50
1.0 wt % MoS_2/Nafion	6.72	±0.95	29.90	±0.94
0.5 wt % MoS_2+Nafion	17.18	±0.83	26.55	±0.87

4. CONCLUSIONS

MoS_2/Nafion composite membranes with extremely enhanced transport properties; that is, both high proton conductivity and reduced methanol permeability are successfully obtained via a selective-growth approach. During the membrane preparation, the strong interactions between the Mo precursor ($(NH_4)_2MoS_4$) and Nafion's sulfonic groups in a suitable solvent environment (DMF) probably lead to the selective growth of MoS_2 flakes mainly around the ionic cluster domains. This process significantly promotes the aggregation and hence leads to better connectivity of these ionic clusters, which greatly favors the increase in proton conductivity of the resultant PEMs. Meanwhile, the existence of MoS_2 flakes in those ionic channels could effectively increase the tortuosity of the membrane and prevent methanol transporting through the membrane, contributing to the dramatic decrease in methanol

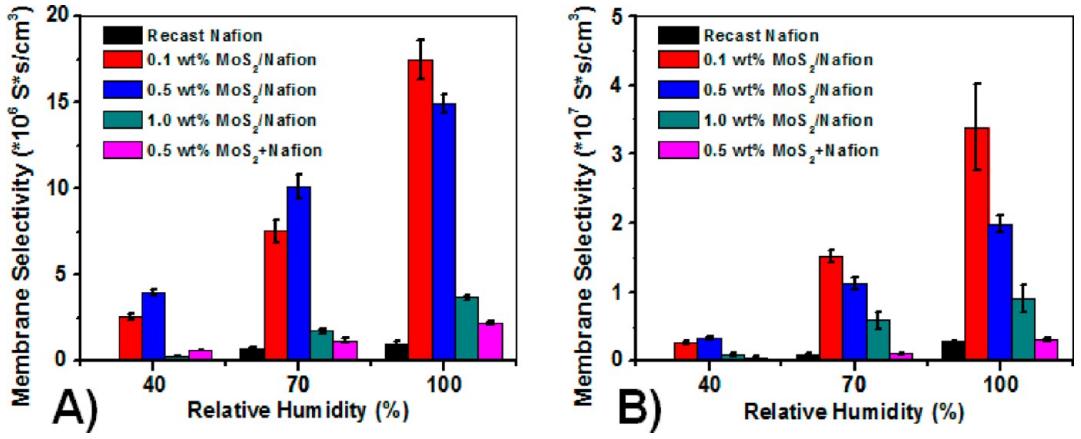

Figure 7. Membrane selectivity of the recast Nafion, the 0.1−1.0 wt % MoS_2/Nafion composite membranes, and the 0.5 wt % MoS_2+Nafion blending membrane under 25 °C (A) and 50 °C (B). They are calculated based on the proton conductivity data in Figure 6A, B and the methanol permeability data in Table 1.

crossover. This promising strategy applies equally for other TMDs or TMOs, for example, WS_2, offering new degrees of freedom to take full advantage of the fascinating properties of various 2D materials to prepare high-performance PEMs.

■ ASSOCIATED CONTENT

Supporting Information

Schematic illustration of the preparation procedures of these PEMs (Figure S1); SEM images, XRD pattern, and IR spectrum of pristine MoS_2 (Figure S2); EDX, surface FE-SEM images and AFM image of the 0.5 wt % MoS_2/Nafion composite membrane (Figure S3); surface FE-SEM and EDX characterizations of the 0.5 wt % MoS_2+Nafion blending membrane (Figure S4); surface SEM images and XRD pattern of the 2.0 wt % MoS_2/Nafion composite membrane (Figure S5); two more AFM phase images of the recast Nafion membrane and the 0.5 wt % MoS_2/Nafion composite membrane (Figure S6). This material is available free of charge via the Internet at http://pubs.acs.org.

■ AUTHOR INFORMATION

Corresponding Authors

*Tel.: +86-21-65643255. Fax: +86-21-65640293. E-mail: bbtang@fudan.edu.cn.

*Tel.: +86-21-65643255. Fax: +86-21-65640293. E-mail: peiyiwu@fudan.edu.cn.

Notes

The authors declare no competing financial interest.

■ ACKNOWLEDGMENTS

We are very grateful for the financial support of the National Natural Science Foundation of China (NSFC) (No. 21276051), Chinese doctoral fund (20110071130001), the Natural Science Foundation of Shanghai (No. 12ZR1401900), and the National Basic Research Program of China (2009CB930000).

■ REFERENCES

(1) Zhao, Q.; An, Q. F. F.; Ji, Y. L.; Qian, J. W.; Gao, C. J. *J. Membr. Sci.* **2011**, *379*, 19−45.
(2) Contestabile, M.; Offer, G. J.; Slade, R.; Jaeger, F.; Thoennes, M. *Energy Environ. Sci.* **2011**, *4*, 3754−3772.
(3) Mohanapriya, S.; Bhat, S. D.; Sahu, A. K.; Manokaran, A.; Vijayakumar, R.; Pitchumani, S.; Sridhar, P.; Shukla, A. K. *Energy Environ. Sci.* **2010**, *3*, 1746−1756.
(4) Neburchilov, V.; Martin, J.; Wang, H. J.; Zhang, J. J. *J. Power Sources* **2007**, *169*, 221−238.
(5) Zarrin, H.; Higgins, D.; Jun, Y.; Chen, Z. W.; Fowler, M. *J. Phys. Chem. C* **2011**, *115*, 20774−20781.
(6) Argun, A. A.; Ashcraft, J. N.; Hammond, P. T. *Adv. Mater.* **2008**, *20*, 1539−1543.
(7) Winter, M.; Brodd, R. J. *Chem. Rev.* **2004**, *104*, 4245−4269.
(8) Zhao, X.; Yin, M.; Ma, L.; Liang, L.; Liu, C. P.; Liao, J. H.; Lu, T. H.; Xing, W. *Energy Environ. Sci.* **2011**, *4*, 2736−2753.
(9) Mohanapriya, S.; Bhat, S. D.; Sahu, A. K.; Pitchumani, S.; Sridhar, P.; Shukla, A. K. *Energy Environ. Sci.* **2009**, *2*, 1210−1216.
(10) Ponce, M. L.; Prado, L.; Silva, V.; Nunes, S. P. *Desalination* **2004**, *162*, 383−391.
(11) Silva, V. S.; Weisshaar, S.; Reissner, R.; Ruffmann, B.; Vetter, S.; Mendes, A.; Madeira, L. M.; Nunes, S. *J. Power Sources* **2005**, *145*, 485−494.
(12) Choi, B. G.; Huh, Y. S.; Park, Y. C.; Jung, D. H.; Hong, W. H.; Park, H. *Carbon* **2012**, *50*, 5395−5402.
(13) Kumar, R.; Xu, C. X.; Scott, K. *RSC Adv.* **2012**, *2*, 8777−8782.
(14) Liu, Y. L.; Su, Y. H.; Chang, C. M.; Suryani; Wang, D. M.; Lai, J. Y. *J. Mater. Chem.* **2010**, *20*, 4409−4416.
(15) Chen, Z. W.; Holmberg, B.; Li, W. Z.; Wang, X.; Deng, W. Q.; Munoz, R.; Yan, Y. S. *Chem. Mater.* **2006**, *18*, 5669−5675.
(16) Feng, K.; Tang, B. B.; Wu, P. Y. *ACS Appl. Mater. Interfaces* **2013**, *5*, 1481−1488.
(17) Paik, Y.; Kim, S. S.; Han, O. H. *Angew. Chem., Int. Ed.* **2008**, *47*, 94−96.
(18) Chai, Z. L.; Wang, C.; Zhang, H. J.; Doherty, C. M.; Ladewig, B. P.; Hill, A. J.; Wang, H. T. *Adv. Funct. Mater.* **2010**, *20*, 4394−4399.
(19) Kannan, R.; Parthasarathy, M.; Maraveedu, S. U.; Kurungot, S.; Pillai, V. K. *Langmuir* **2009**, *25*, 8299−8305.
(20) Estevez, L.; Kelarakis, A.; Gong, Q. M.; Da'as, E. H.; Giannelis, E. P. *J. Am. Chem. Soc.* **2011**, *133*, 6122−6125.
(21) Sekhon, S. S.; Park, J. S.; Cho, E.; Yoon, Y. G.; Kim, C. S.; Lee, W. Y. *Macromolecules* **2009**, *42*, 2054−2062.
(22) Ran, J.; Wu, L.; Varcoe, J. R.; Ong, A. L.; Poynton, S. D.; Xu, T. W. *J. Membr. Sci.* **2012**, *415*, 242−249.
(23) Geim, A. K.; Novoselov, K. S. *Nat. Mater.* **2007**, *6*, 183−191.
(24) Stankovich, S.; Dikin, D. A.; Dommett, G. H. B.; Kohlhaas, K. M.; Zimney, E. J.; Stach, E. A.; Piner, R. D.; Nguyen, S. T.; Ruoff, R. S. *Nature* **2006**, *442*, 282−286.
(25) Coleman, J. N.; Lotya, M.; O'Neill, A.; Bergin, S. D.; King, P. J.; Khan, U.; Young, K.; Gaucher, A.; De, S.; Smith, R. J.; Shvets, I. V.; Arora, S. K.; Stanton, G.; Kim, H. Y.; Lee, K.; Kim, G. T.; Duesberg, G. S.; Hallam, T.; Boland, J. J.; Wang, J. J.; Donegan, J. F.; Grunlan, J. C.;

Moriarty, G.; Shmeliov, A.; Nicholls, R. J.; Perkins, J. M.; Grieveson, E. M.; Theuwissen, K.; McComb, D. W.; Nellist, P. D.; Nicolosi, V. *Science* **2011**, *331*, 568−571.
(26) Liu, J. Q.; Zeng, Z. Y.; Cao, X. H.; Lu, G.; Wang, L. H.; Fan, Q. L.; Huang, W.; Zhang, H. *Small* **2012**, *8*, 3517−3522.
(27) Mancinelli, K. C. B.; Lisboa, F. D.; Soares, J. F.; Zawadzki, S. F.; Wypych, F. *Mater. Chem. Phys.* **2013**, *137*, 764−771.
(28) Zhou, K. Q.; Jiang, S. H.; Bao, C. L.; Song, L.; Wang, B. B.; Tang, G.; Hu, Y.; Gui, Z. *RSC Adv.* **2012**, *2*, 11695−11703.
(29) Cao, Y.; Zhang, J.; Feng, J.; Wu, P. *ACS Nano* **2011**, *5*, 5920−5927.
(30) Jiang, Z. Q.; Zhao, X. S.; Manthiram, A. *Int. J. Hydrogen Energy* **2013**, *38*, 5875−5884.
(31) Cao, Y.; Lai, Z.; Feng, J.; Wu, P. *J. Mater. Chem.* **2011**, *21*, 9271−9278.
(32) Cao, Y.; Feng, J.; Wu, P. *Carbon* **2010**, *48*, 3834−3839.
(33) Feng, K.; Cao, Y.; Wu, P. *J. Mater. Chem.* **2012**, *22*, 11455−11457.
(34) Sun, Y. Q.; Wu, Q. O.; Shi, G. Q. *Energy Environ. Sci.* **2011**, *4*, 1113−1132.
(35) Huang, C.; Li, C.; Shi, G. *Energy Environ. Sci.* **2012**, *5*, 8848−8868.
(36) Li, Y. G.; Wang, H. L.; Xie, L. M.; Liang, Y. Y.; Hong, G. S.; Dai, H. J. *J. Am. Chem. Soc.* **2011**, *133*, 7296−7299.
(37) Wang, T. Y.; Liu, L.; Zhu, Z. W.; Papakonstantinou, P.; Hu, J. B.; Liu, H. Y.; Li, M. X. *Energy Environ. Sci.* **2013**, *6*, 625−633.
(38) Vrubel, H.; Merki, D.; Hu, X. L. *Energy Environ. Sci.* **2012**, *5*, 6136−6144.
(39) Merki, D.; Hu, X. L. *Energy Environ. Sci.* **2011**, *4*, 3878−3888.
(40) Zhang, R.; Wolters, L.; Weidner, J. W. *Int. J. Hydrogen Energy* **2012**, *37*, 2935−2939.
(41) Zhang, R.; Weidner, J. W. *ECS Trans.* **2010**, *28*, 51−63.
(42) Wang, H. L.; Robinson, J. T.; Diankov, G.; Dai, H. J. *J. Am. Chem. Soc.* **2010**, *132*, 3270−3271.
(43) Wang, H. L.; Cui, L. F.; Yang, Y. A.; Casalongue, H. S.; Robinson, J. T.; Liang, Y. Y.; Cui, Y.; Dai, H. J. *J. Am. Chem. Soc.* **2010**, *132*, 13978−13980.
(44) Altavilla, C.; Sarno, M.; Ciambelli, P. *Chem. Mater.* **2011**, *23*, 3879−3885.
(45) Lai, H. J.; Wang, Z. W.; Wu, P. Y.; Chaudhary, B. I.; Sengupta, S. S.; Cogen, J. M.; Li, B. *Ind. Eng. Chem. Res.* **2012**, *51*, 9365−9375.
(46) Wang, M. Y.; Wu, P. Y.; Sengupta, S. S.; Chadhary, B. I.; Cogen, J. M.; Li, B. *Ind. Eng. Chem. Res.* **2011**, *50*, 6447−6454.
(47) Tang, B. B.; Wu, P. Y. *Vib. Spectrosc.* **2009**, *51*, 65−71.
(48) Tang, B. B.; Wu, P. Y.; Siesler, H. W. *J. Phys. Chem. B* **2008**, *112*, 2880−2887.
(49) Balik, C. M.; Simendinger, W. H. *Polymer* **1998**, *39*, 4723−4728.
(50) Fieldson, G. T.; Barbari, T. A. *Polymer* **1993**, *34*, 1146−1153.
(51) Hajatdoost, S.; Yarwood, J. *J. Chem. Soc., Faraday Trans.* **1997**, *93*, 1613−1620.
(52) Pereira, M. R.; Yarwood, J. *J. Chem. Soc., Faraday Trans.* **1996**, *92*, 2737−2743.
(53) Dhoot, G.; Auras, R.; Rubino, M.; Dolan, K.; Soto Valdez, H. *Polymer* **2009**, *50*, 1470−1482.
(54) Fieldson, G. T.; Barbari, T. A. *AIChE J.* **1995**, *41*, 795−804.
(55) Braun, J. L.; Kadla, J. F. *Biomacromolecules* **2005**, *6*, 152−160.
(56) Cava, D.; Sammon, C.; Lagaron, J. M. *J. Appl. Polym. Sci.* **2007**, *103*, 3431−3437.
(57) Fieldson, G. T.; Barbari, T. A. *Polymer* **1993**, *34*, 1146−1153.
(58) O'Neill, A.; Khan, U.; Coleman, J. N. *Chem. Mater.* **2012**, *24*, 2414−2421.
(59) Hu, K. H.; Hu, X. G. *Mater. Sci. Technol.* **2009**, *25*, 407−414.
(60) Chen, W. F.; Wu, J. S.; Kuo, P. L. *Chem. Mater.* **2008**, *20*, 5756−5767.
(61) Yasuda, T.; Nakamura, S.; Honda, Y.; Kinugawa, K.; Lee, S. Y.; Watanabe, M. *ACS Appl. Mater. Interfaces* **2012**, *4*, 1783−1790.
(62) Affoune, A. M.; Yamada, A.; Umeda, M. *J. Power Sources* **2005**, *148*, 9−17.
(63) Fu, L. C.; Xiao, G. Y.; Yan, D. Y. *ACS Appl. Mater. Interfaces* **2010**, *2*, 1601−1607.